

Performance Evaluation and Parametric Optimum Criteria of an Irreversible Molten Carbonate Fuel Cell-Heat Engine Hybrid System

Houcheng Zhang, Guoxing Lin[§], Jincan Chen^{*}

Department of Physics, Xiamen University, Xiamen 361005, People's Republic of China

E-mail: [§gxin@xmu.edu.cn](mailto:gxin@xmu.edu.cn), [*jcchen@xmu.edu.cn](mailto:jcchen@xmu.edu.cn)

Received: 1 August 2011 / Accepted: 2 September 2011 / Published: 1 October 2011

The model of a hybrid system composed of a molten carbonate fuel cell (MCFC) and a heat engine is presented, in which multi-irreversibilities such as overpotentials in the electrochemical reaction, heat leak from the MCFC to the environment, non-perfect regeneration in the regenerator, and finite-rate heat transfer in the heat engine are taken into account. Expressions for the efficiency and power output of the system are analytically derived, from which the general characteristics of the hybrid system are revealed and the optimum criteria of some main parameters such as the current density, efficiency and power output are determined. The influence of the irreversible losses on the performance of the hybrid system is discussed. Moreover, a multi-objective function including both the efficiency and the power output is put forward and used to further subdivide the optimally operating region of the hybrid system. The results obtained here are very general and may be directly used to derive the various interesting conclusions of the hybrid systems operated under different special cases.

Keywords: Molten carbonate fuel cell; Heat engine; Hybrid system; Irreversibility; Optimum analysis

1. INTRODUCTION

The dual effects of the limited fossil fuel sources and environment pollution have shown the requirement of innovative energy generation systems to not only increase efficiency but also reduce harmful emissions. The fuel cell is an electrochemical energy conversion system which directly converts chemical energy in a fuel to electricity. This results in high efficiency and low pollutant emissions in comparison with traditional fossil-based energy conversion devices [1-6]. Among the various fuel cells, the molten carbonate fuel cell (MCFC) is very promising because of its fuel flexibility and high operating temperature [7-10]. The high temperature operating characteristics

provide the possibility of cogeneration with other types of power generators such as gas turbines [11-14] or heat engines [15-18], so that the performance of the MCFC hybrid systems can be enhanced.

Since the concept of fuel cell-heat engine hybrid systems was proposed, a number of theoretical and experimental investigations have been carried out, which include the thermodynamic analysis [15-17], the finding promising bottoming cycles [18, 19], the plant configurations [20, 21], and so on [22, 23]. However, what is the upper bound of performance for the MCFC hybrid system? It is still an interesting problem that has not solved yet. It is well known that for the various heat engines operated at between two heat reservoirs, the efficiency obtained by the Carnot heat engine is maximum. Thus, it will be an available method to theoretically determine the maximum efficiency and power output of the MCFC-heat engine hybrid system if the Carnot heat engine is connected with the MCFC.

In the present paper, the performance and the parametric chosen criteria of the MCFC-heat engine hybrid system will be analyzed and discussed systematically. The concrete contents are arranged as follows.

In Sec. 2, the model of the MCFC-heat engine hybrid system consisting of an MCFC, a regenerator and a heat engine is established and each assembly unit in the hybrid system will be mathematically described. The efficiency and the power output of the hybrid system are analytically derived.

In Sec. 3, the general performance characteristics of the hybrid system are revealed and the optimum criteria of some main performance parameters are determined. A multi-objective function is used to further expound how to give consideration to both the efficiency and the power output of the hybrid system.

In Sec. 4, the effects of some synthesized parameters representing the irreversible losses on the performance of the hybrid system are discussed in details. Some significant results for several special cases are directly obtained. Finally, some important conclusions are summarized.

2. DEPICTION OF AN IRREVERSIBLE MCFC-HEAT ENGINE HYBRID SYSTEM

Figure 1 shows the schematic diagram of an MCFC-heat engine hybrid system composed of an MCFC, a heat engine, and a regenerator, where T_0 is the environment temperature, T is the working temperature of the MCFC, P_M and P_H are the power outputs of the MCFC and heat engine, q_h is the rate of heat transfer between the MCFC and the heat engine, q_l is the rate of heat transfer between the heat engine and the environment, q_{Loss} is the rate of heat losses from the MCFC to the environment. In Fig. 1, the MCFC acts as the high-temperature heat reservoir of the heat engine for a further power production and the regenerator in the hybrid system is to preheat the incoming reactants by means of the heat in the high temperature products. By using such a hybrid system, the heat produced in the MCFC can be efficiently utilized, and consequently, the performance of the MCFC system can be improved. Below, every assembly unit in the hybrid system will be, respectively, discussed in the next several subsections.

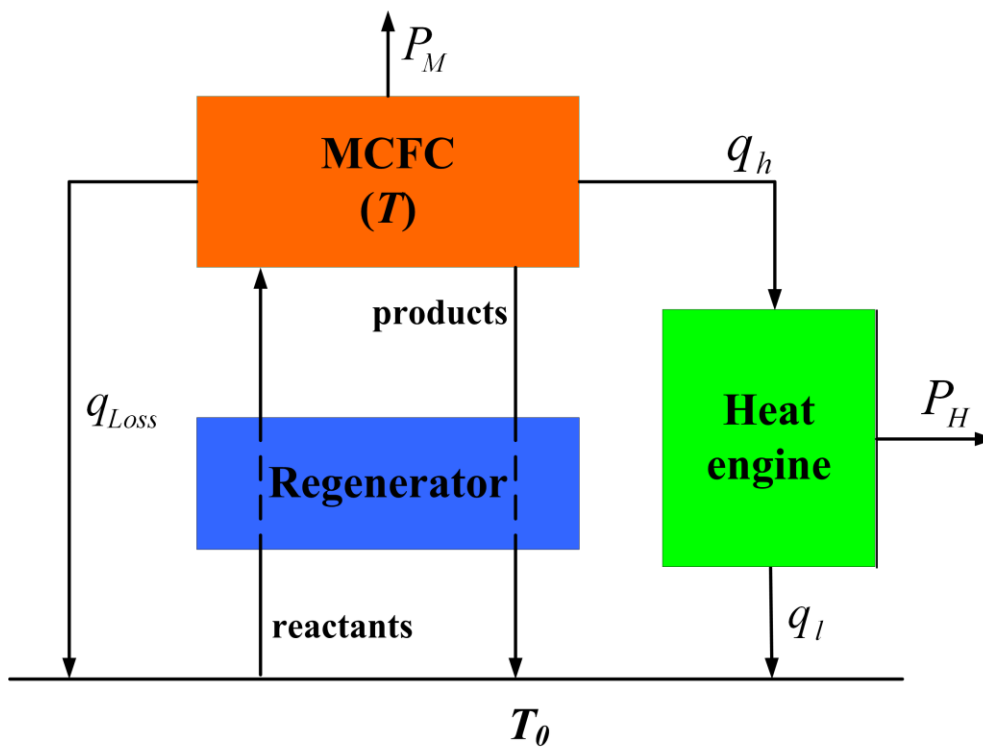


Figure 1. The schematic diagram of an MCFC-heat engine hybrid system.

2.1 An irreversible MCFC

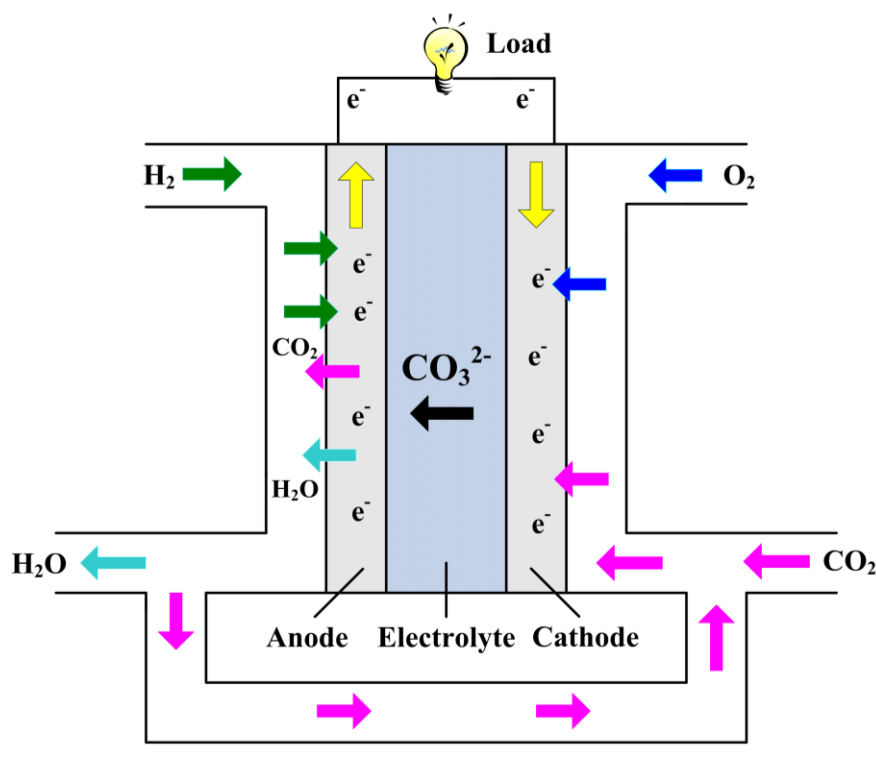
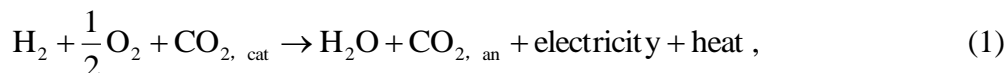


Figure 2. The schematic diagram of an MCFC.

Many researchers have elaborately demonstrated the operating mechanism of the MCFC [7, 9, 24-27]. Here, we only give a simple description for an MCFC. As shown in Fig. 2, an MCFC is operated by introducing hydrogen to the anode and oxygen and carbon dioxide (if necessary) to the cathode, respectively. At the anode hydrogen reacts with carbonate ions available in the carbonate electrolyte into water and carbon dioxide and releases electrons to the external electric circuit, i.e., $\text{H}_2 + \text{CO}_3^{2-} \rightarrow \text{H}_2\text{O} + \text{CO}_2 + 2\text{e}^-$. At the cathode oxygen reacts with carbon dioxide and electrons into carbonate ions, i.e., $\frac{1}{2}\text{O}_2 + \text{CO}_2 + 2\text{e}^- \rightarrow \text{CO}_3^{2-}$. The overall electrochemical reaction is



where subscripts “an” and “cat” indicate “anode” and “cathode”, respectively. To sustain the total electrochemical reaction, the produced carbon dioxide is transported from the anode to the cathode while the produced carbonate ions flow from the cathode to the anode. It should be pointed out that the overall reaction is exo-energetic. These energies include an electric part, which is consumed in the external electric circuit, and a thermal part, which can be used for further power production by the heat engine, i.e., $-\Delta H = -\Delta G - T\Delta S$, where $-\Delta H$ is the total energy released by the reaction, $-\Delta G$ is the electric part and $-T\Delta S$ is the thermal part.

According to Faraday’s law, hydrogen consumption rate in the electrochemical reaction is determined by $\dot{q}_{\text{H}_2} = I/(n_e F)$, where I is the operating electric current, n_e is the number of electrons, and F is Faraday’s constant [28, 29]. Thus, the maximum possible energy (both electrical and thermal) released by the reactions is [15]

$$-\Delta \dot{H} = -\dot{q}_{\text{H}_2} \Delta h^0 = -\frac{I \Delta h^0}{n_e F}, \quad (2)$$

where Δh^0 is the standard molar enthalpy change and can be calculated from the data in Refs. [28, 30-32].

It is well known that the measured open circuit voltage U_{cell} in a practical fuel cell is always lower than the ideal reversible voltage U_0 determined by Nernst equation [25, 33-35] because there exist some irreversible losses resulting from the anode overpotential U_{an} , cathode overpotential U_{cat} , and ohmic overpotential U_{ohm} . The three overpotentials can be, respectively, expressed as [24, 26, 34, 36]:

$$U_{\text{an}} = 2.27 \times 10^{-9} j \exp\left(\frac{E_{\text{act,an}}}{RT}\right) P_{\text{H}_2,\text{an}}^{-0.42} P_{\text{CO}_2,\text{an}}^{-0.17} P_{\text{H}_2\text{O},\text{an}}^{-1.0}, \quad (3)$$

$$U_{\text{cat}} = 7.505 \times 10^{-10} j \exp\left(\frac{E_{\text{act,cat}}}{RT}\right) P_{\text{O}_2,\text{cat}}^{-0.43} P_{\text{CO}_2,\text{cat}}^{-0.09}, \quad (4)$$

and

$$U_{ohm} = 0.5 \times 10^{-4} j \exp \left[3016 \left(\frac{1}{T} - \frac{1}{923} \right) \right], \tag{5}$$

where j is the operating current density; R is the universal gas constant; E_{act} is the activation energy, and p_k are the partial pressures of species k at the anode or cathode. It should be pointed out that the anode overpotential can be achieved its minimum when the anode gas inlet compositions are optimally chosen. By using numerical calculation, the concrete values of the optimal anode gas compositions under the different H_2 concentrations are listed in Table 1. Furthermore, the cathode overpotential decreases when the O_2 and/or CO_2 concentrations are increased.

Table 1. The optimal anode gas compositions under the different H_2 concentrations.

| H_2 concentration (%) | CO_2 concentration (%) | H_2O concentration (%) |
|-------------------------------|--------------------------------|--------------------------------|
| 50 | 7.2 | 42.8 |
| 60 | 5.8 | 34.2 |
| 70 | 4.4 | 25.6 |
| 80 | 2.8 | 17.2 |

With the help of the above analysis, the efficiency and power output of an irreversible MCFC may be, respectively, expressed as

$$\eta_M = \frac{P_M}{-\Delta \dot{H}} = \frac{n_e F (U_0 - U_{an} - U_{cat} - U_{ohm})}{-\Delta h^0} \tag{6}$$

and

$$P_M = U_{cell} I = (U_0 - U_{an} - U_{cat} - U_{ohm}) I, \tag{7}$$

where $I = jA$ is the electric current through the MCFC and A is the effective surface area of the MCFC.

2.2 An irreversible regenerator

The regenerator in the hybrid system acted as a heat exchanger, heating the inlet reactants from the ambient temperature to the temperature of MCFC by using the high-temperature products. When the regenerative efficiency ε of the regenerator is equal to 1, the regenerative process is ideal and the additional heat is unnecessary. It should be pointed out that owing to the existence of the thermal resistance, the regenerative losses are inevitable. It is reasonable to assume that the rate of the

regenerative losses is directly proportional to the temperature difference between the MCFC and the environment [37, 38], i.e.,

$$q_{re} = U_{re} A_{re} (1 - \varepsilon)(T - T_0), \tag{8}$$

where U_{re} and A_{re} are, respectively, the heat-transfer coefficient and heat-transfer area between the regenerator and the environment. In order to replenish the heat losses in the regenerative process, the additional heat may be usually transferred from the MCFC at temperature T to the inlet reactants in the regenerator in time so that the export temperature of the inlet reactants is ensured to attain the working temperature of the MCFC.

2.3 An endoreversible heat engine

For the heat engine in the hybrid system, the MCFC working at temperature T can be taken as to be a high temperature heat reservoir and the environment is a low temperature reservoir. Thus, we can use a Carnot heat engine to further convert the heat produced in the MCFC into power. For the sake of simplification, the cyclic model of the heat engine is assumed to be endoreversible [15, 39] and heat transfer between the heat engine and the heat reservoirs obeys Newton's law [15, 40]. It has been proved that for given rate of heat input q_h and total heat-transfer area A_h of the heat engine, when the condition $A_1 / A_2 = \sqrt{U_2 / U_1}$ is satisfied, the efficiency of the heat engine may be expressed as [15, 40, 41]

$$\eta_H = 1 - T_0 / (T - q_h / K), \tag{9}$$

where $K = U_1 U_2 A_h / (\sqrt{U_1} + \sqrt{U_2})^2$ is a parameter to measure the irreversibility of finite-rate heat transfer in the heat engine, $A_h = A_1 + A_2$, A_1 and A_2 are the heat-transfer areas between the heat engine and the two heat reservoirs, and U_1 and U_2 are the heat-transfer coefficients between the heat engine and the two heat reservoirs.

According to Fig.1, one can derive the rate of heat input from the MCFC to the heat engine as

$$q_h = -\Delta \dot{H} - P_M - q_{re} - q_{Loss}, \tag{10}$$

where the heat loss q_{Loss} from the MCFC to the environment may be expressed as [40, 42, 43]

$$q_{Loss} = U_3 A_3 (T - T_0), \tag{11}$$

U_3 is the convective and/or conductive heat-leak coefficient, and A_3 is the effective heat-transfer area.

By using Eqs. (8)-(11), the efficiency and power output of the heat engine may be, respectively, expressed as

$$\eta_H = 1 - \frac{1}{T/T_0 - m_1[(1 - \eta_M)j - m_2(T/T_0 - 1)]} \quad (12)$$

and

$$P_H = q_h \eta_H = \frac{-A\Delta h^0}{n_e F} [(1 - \eta_M)j - m_2(T/T_0 - 1)] \left\{ 1 - \frac{1}{T/T_0 - m_1[(1 - \eta_M)j - m_2(T/T_0 - 1)]} \right\}, \quad (13)$$

where $m_1 = -\frac{A\Delta h^0}{n_e FKT_0}$ and $m_2 = \frac{U_3 A_3 + U_{re} A_{re} (1 - \varepsilon)}{-A\Delta h^0 / (n_e F T_0)}$.

2.4 The efficiency and power output of the hybrid system

Table 2. Parameters used in the modeling of the MCFC-heat engine hybrid system [24, 34, 36].

| Parameter | Value |
|---|---------|
| Faraday constant, F (C mol ⁻¹) | 96,485 |
| Number of electrons, n_e | 2 |
| Universal gas constant, R (J mol ⁻¹ K ⁻¹) | 8.314 |
| Operating temperature, T (K) | 893 |
| Temperature of environment, T_0 (K) | 298.15 |
| Operating pressure, p (atm) | 1 |
| Partial pressure of H ₂ in the anode, $p_{H_2,an}$ (atm) | 0.60 |
| Partial pressure of O ₂ in the cathode, $p_{O_2,cat}$ (atm) | 0.08 |
| Partial pressure of N ₂ in the cathode, $p_{N_2,cat}$ (atm) | 0.59 |
| Partial pressure of CO ₂ in the cathode, $p_{CO_2,cat}$ (atm) | 0.08 |
| Partial pressure of H ₂ O in the cathode, $p_{H_2O,cat}$ (atm) | 0.25 |
| Activation energy in the anode, $E_{act,an}$ (J mol ⁻¹) | 53,500 |
| Activation energy in the cathode, $E_{act,cat}$ (J mol ⁻¹) | 77,300 |
| Constant, m_1 (m ² A ⁻¹) | 0.00033 |
| Constant, m_2 | 1 |

By using Eqs. (2), (6), (7), (12), and (13), the efficiency and power output of the hybrid system can be, respectively, expressed as

$$\eta = \frac{P_M + P_H}{-\dot{\Delta H}} = \eta_M + [1 - \eta_M - \frac{m_2(T/T_0 - 1)}{j}] \times \left[1 - \frac{1}{T/T_0 - m_1[(1 - \eta_M)j - m_2(T/T_0 - 1)]} \right] \quad (14)$$

and

$$P = P_M + P_H = -\frac{jA\Delta h^0}{n_e F} \eta. \quad (15)$$

It is seen from Eqs. (14) and (15) that the performance of the MCFC-heat engine hybrid system depends on a set of thermodynamic and electrochemical parameters such as the working temperature, current density, synthesized parameters m_i ($i=1, 2$), partial pressures of electrodes gas compositions, and so on. Below, numerical calculations are carried out based on the data summarized in Table 2, and these parameters are kept constant unless mentioned specifically.

3. GENERAL PERFORMANCE CHARACTERISTICS AND PARAMETRIC OPTIMUM CRITERIA

Using Eqs. (6), (7), and (12)-(15), one can generate the curves of the efficiency and power output of the MCFC, heat engine and hybrid system varying with the current density, as shown in Figs. 3 and 4.

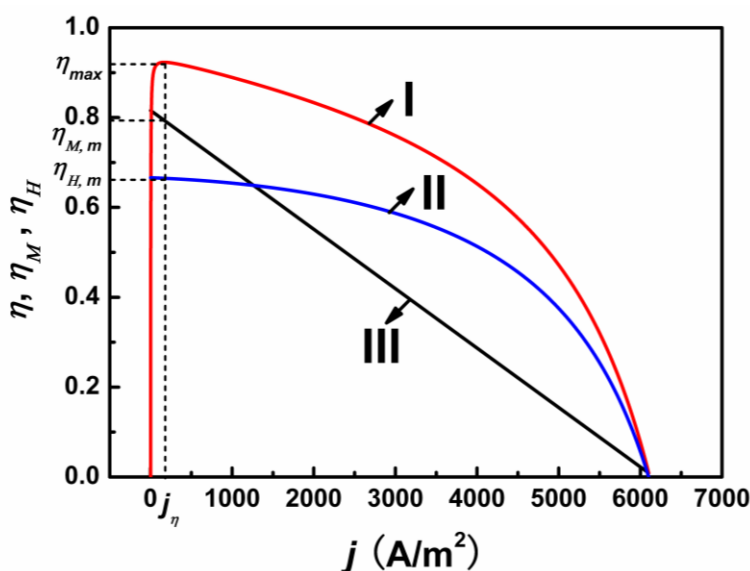


Figure 3. The curves of the efficiencies of the hybrid system, heat engine, and MCFC varying with the current density, where j_η is the current density at the maximum efficiency η_{max} of the hybrid system, $\eta_{M,m}$ and $\eta_{H,m}$ are the efficiencies of the MCFC and heat engine in the hybrid system at the maximum η_{max} , and curves I, II and III correspond to the cases of the hybrid system, heat engine, and MCFC, respectively.

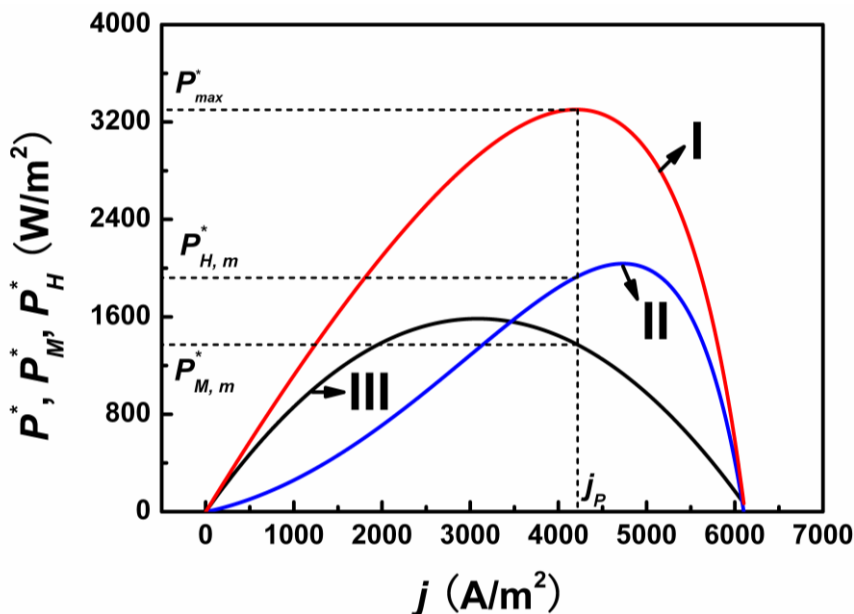


Figure 4. The curves of the power densities of the hybrid system, heat engine, and MCFC varying with the current density, where j_P is the current densities at the maximum power density P_{max}^* , $P_{H,m}^*$ and $P_{M,m}^*$ are the power densities of the heat engine and MCFC in the hybrid system at the maximum P_{max}^* , and curves I, II, and III correspond to the same cases as those in Fig. 3.

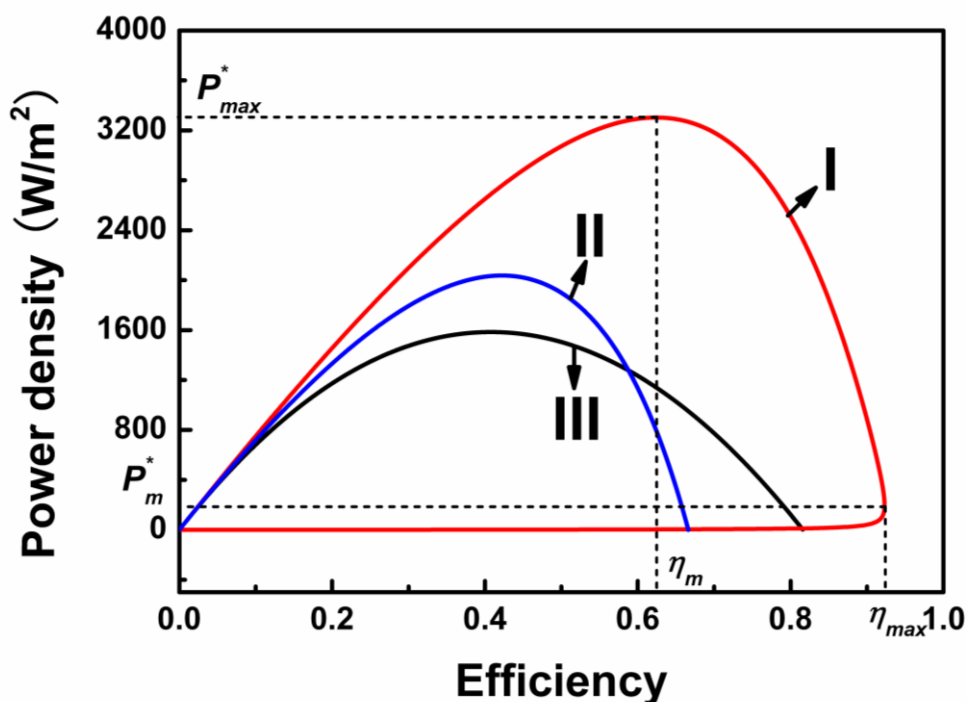


Figure 5. The power density versus efficiency curves of the hybrid system, heat engine, and MCFC, where curve I, II, and III correspond to the same cases as those in Fig.3.

It is clearly seen from Figs. 3 and 4 that there are a maximum efficiency η_{\max} and a maximum power density P_{\max}^* for the hybrid system and the corresponding current densities are j_η and j_p , respectively. It is also seen from Figs. 3 and 4 that in the region of $j < j_\eta$, both the efficiency and the power output of the hybrid system will decrease as the current density j is decreased, while in the region of $j > j_p$, both the efficiency and power output of the hybrid system will decrease as the current density j is increased.

Obviously, the regions of $j < j_\eta$ and $j > j_p$ are not the optimally operating region of the hybrid system. Thus, the optimally operating region of the current density j for the MCFC-heat engine hybrid system should be determined by

$$j_\eta \leq j \leq j_p. \tag{16}$$

To further understand the performance characteristics of the hybrid system, one can plot the power density versus efficiency curves of the hybrid system, as shown in Fig. 5. According to the optimum criterion of the current density and Fig. 5, one can further determine the optimum regions for the efficiency and power output as

$$\eta_m \leq \eta \leq \eta_{\max} \tag{17}$$

and

$$P_m \leq P \leq P_{\max}, \tag{18}$$

where η_m and P_m are, respectively, the efficiency at the maximum power output and the power output at the maximum efficiency. It is clearly seen from Figs. 3-5 that in the optimally operating region, the efficiency and power output of the hybrid system are always larger than those of the MCFC or heat engine. It shows once again that the application of the hybrid system may effectively improve the performance of the MCFC system.

It should be pointed out that when the hybrid system is operated in the optimum region, the power output will increase as the efficiency is decreased, and vice versa. Generally, the power output P_m is very small when the hybrid system achieves its maximum efficiency η_{\max} and the efficiency η_m is not large compared with η_{\max} when the hybrid system achieves its maximum power output P_{\max} . Thus, the problem how to reasonably choose both the efficiency and power output in the optimal region of $j_\eta \leq j \leq j_p$ will become very important in the practical optimum design and operation of the hybrid system. For this reason, we may introduce a multi-objective function which is defined as the product of the efficiency with a weighting factor and power output [44-46], i.e.,

$$Z_\lambda = \eta^\lambda P \tag{19}$$

where λ is the weighting factor which can be chosen according to the different requirements for the efficiency and power output of the MCFC-heat engine hybrid system and $0 \leq \lambda < \infty$. When $0 < \lambda < \infty$, the multi-objective function is related to not only the efficiency and power output but also the concrete value of the weighting factor λ . In such a case, the multi-objective function is neither the efficiency nor the power output. When $\lambda = 0$, the multi-objective function becomes one objective function, i.e., the power output. When $\lambda \rightarrow \infty$, the multi-objective function tends to zero, but it may be rewritten as $Z_\lambda^{1/\lambda} = \eta P^{1/\lambda}$, which is the other objective function, i.e., the efficiency. When one pays equal attention to both the efficiency and power output, one can choose $\lambda = 1$. Below, we will take $\lambda = 1$ as an example to discuss the choice problem of the optimal current density.

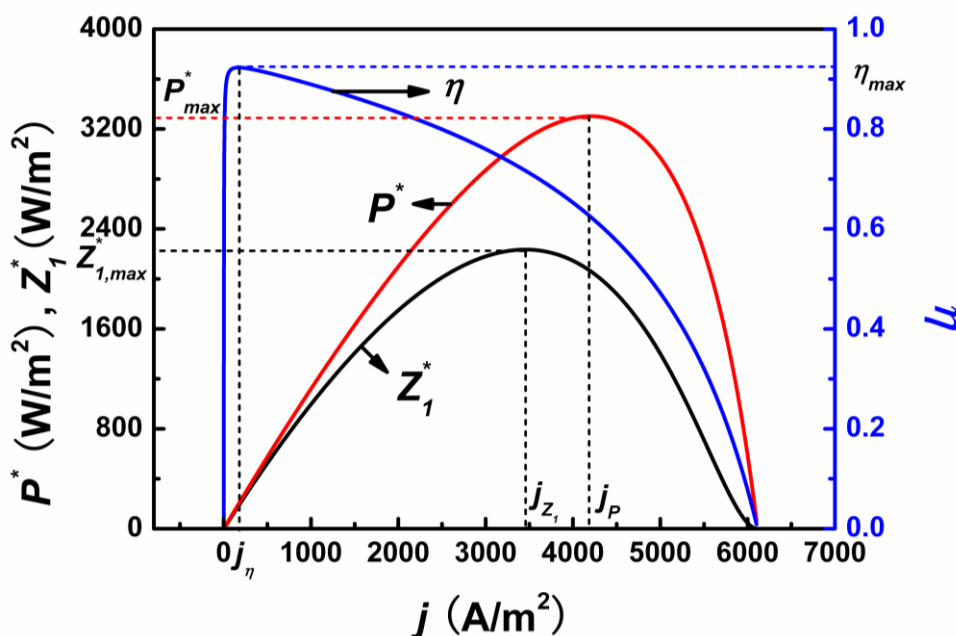


Figure 6. The curves of the efficiency, power density and multi-objective function of the hybrid system varying with the current density, where j_η , j_P and j_{Z_1} are the current densities at the maximum efficiency, power density and multi-objective function, respectively.

According to Eqs. (14), (15), and (19), we can generate the curve of $Z_1^* \sim j$, as shown in Fig. 6, where $Z_1^* = Z_1 / A$ and j_{Z_1} is the current density corresponding to $Z_{1,max}^*$. It is seen from Fig. 6 that Z_1^* first increases and then decreases with the increase of the current density. This means that there always exists a maximum for Z_1^* . Fig. 6 clearly shows that $j_\eta \leq j_{Z_1} \leq j_P$. Thus, the optimal operation region $j_\eta \leq j \leq j_P$ can be subdivided according to the different requirements for both the efficiency and the power output. If more attention is emphasized on the efficiency than on the power output, the optimal operation region of the current density should be

$$j_\eta \leq j \leq j_{Z_1} \tag{20}$$

If more attention is paid on the power output than on the efficiency, the optimal operation region of current density should be

$$j_{Z_1} \leq j \leq j_P \tag{21}$$

4. DISCUSSION

4.1 Effects of the operating temperature T

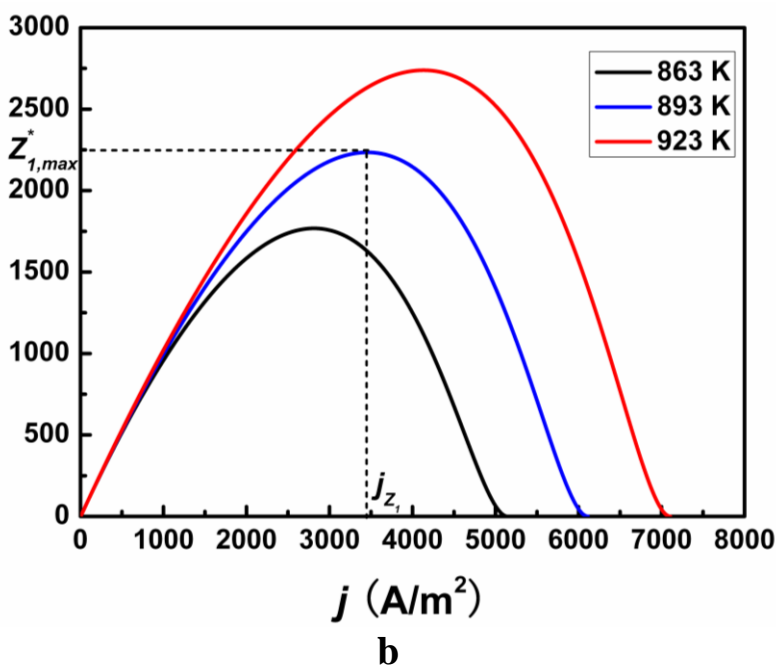
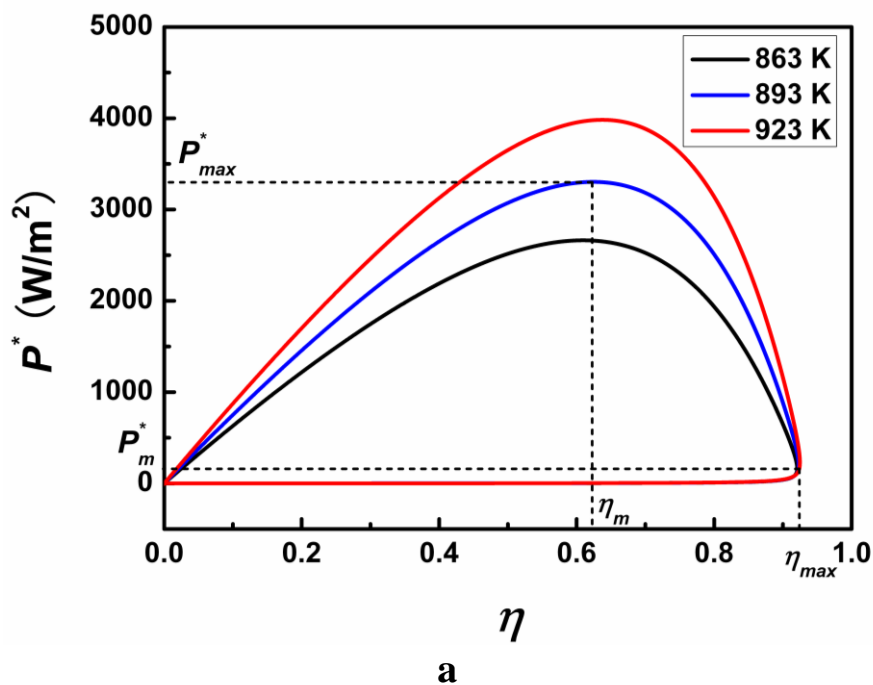


Figure 7. The effect of the operating temperature on (a) the performance of the hybrid system (b) the multi-objective function.

The operating temperature of the system is an important factor because it directly affects the reversible potential as well as the anode, cathode, and ohm overpotentials of the fuel cell. Fig. 7 clearly shows the effects of the operating temperature on the performance of the hybrid system and the multi-objective function.

It can be seen from the Fig. 7 (a) that the maximum power output and its corresponding efficiency as well as the maximum efficiency and its corresponding power output increase as the operating temperature is increased. Fig. 7 (b) shows that the maximum multi-objective function and its corresponding current density increased as the operating temperature is increased. At higher operating temperatures, the electrodes of MCFC are more reactive and the mass transfer within the fuel cell is improved, which result in a net decrease in the overpotentials and a net increase in the reversible potential. Furthermore, the performance of the heat engine is naturally enhanced as the operating temperature T is increased. Thus, the higher the operating temperature of the MCFC-heat engine hybrid system is, the larger the efficiency, power output, and multi-objective function.

4.2 Effects of m_1 and m_2

(1) When $m_1 = 0$, i.e., $K \rightarrow \infty$, the influence of the finite-rate heat transfer irreversibility between the heat engine and the heat reservoirs is negligible. In such a case, Eqs. (12), (14) and (15) may be, respectively, simplified as

$$\eta_H = 1 - \frac{T_0}{T} = \eta_C, \tag{22}$$

$$\eta = \eta_M + \left[1 - \eta_M - \frac{m_2(T/T_0 - 1)}{j} \right] \eta_C, \tag{23}$$

and

$$P = -\frac{jA\Delta h^0}{n_e F} \left\{ \eta_M + \left[1 - \eta_M - \frac{m_2(T/T_0 - 1)}{j} \right] \eta_C \right\}, \tag{24}$$

where η_C is the Carnot efficiency. The power output versus efficiency curve of the hybrid system is shown by curve I in Fig. 8. When $m_1 > 0$, the efficiency and power output of the hybrid system are of monotonically decreasing functions of m_1 .

(2) When $m_2 = 0$, the heat leak from the MCFC to the environment and the irreversible losses in the regenerator are negligible. In such a case, Eqs. (12), (14), and (15) may be, respectively, simplified as

$$\eta_H = 1 - \frac{1}{T/T_0 - jm_1(1 - \eta_M)}, \tag{25}$$

$$\eta = \eta_M + (1 - \eta_M) \left[1 - \frac{1}{T/T_0 - jm_1(1 - \eta_M)} \right], \tag{26}$$

and

$$P = -\frac{jA\Delta h^0}{n_e F} \left\{ \eta_M + (1 - \eta_M) \left[1 - \frac{1}{T/T_0 - jm_1(1 - \eta_M)} \right] \right\}. \tag{27}$$

The power output versus efficiency curve of the hybrid system is shown by curve II in Fig. 8. When $m_2 > 0$, the efficiency and power output of the hybrid system are of monotonically decreasing functions of m_2 .

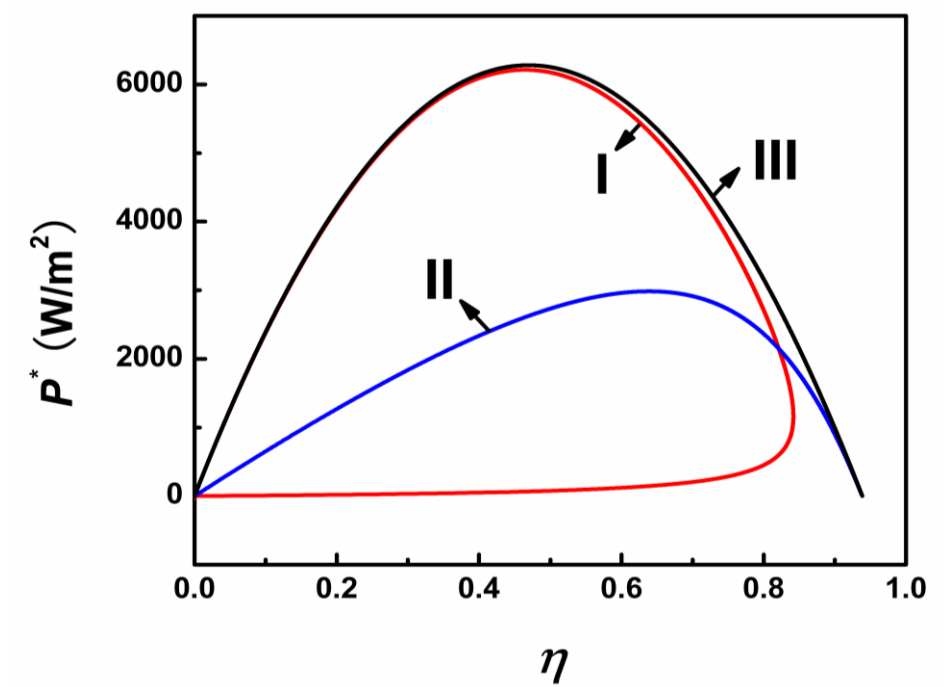


Figure 8. The power density versus efficiency curves of the hybrid system under different conditions, where η_m and P_m^* are the efficiency at the maximum power output P_{\max}^* and the power output at the maximum efficiency η_{\max} , respectively. Curves I, II, and III correspond to the three special cases: $m_1 = 0$ and $m_2 = 40$, $m_1 = 0.00045$ and $m_2 = 0$, and $m_1 = 0$ and $m_2 = 0$, respectively.

(3) When $m_1 = 0$ and $m_2 = 0$, the finite-rate heat transfer irreversibility between the heat engine and the heat reservoirs, the heat leak from the MCFC to the environment, and the heat loss in the regenerator are negligible. In such a case, Eqs. (23) and (24) or Eqs. (26) and (27) can be further simplified as

$$\eta = \eta_M + (1 - \eta_M)\eta_C \quad (28)$$

and

$$P = -\frac{jA\Delta h^0}{n_e F} [\eta_M + (1 - \eta_M)\eta_C], \quad (29)$$

respectively. The power output versus efficiency curve of the hybrid system is shown by curve III in Fig. 8. In a practical MCFC-heat engine hybrid system, $m_1 > 0$ and $m_2 > 0$. The general characteristics of the hybrid system are shown in Figs. 3-7.

5. CONCLUSIONS

With the help of the model of an MCFC-heat engine hybrid system including multi-irreversibilities such as overpotentials in the electrochemical reaction, heat leak from the MCFC to the environment, non-perfect regeneration in the regenerator, finite-rate heat transfer in the heat engine, expressions for the efficiency and power output of the hybrid system are analytically derived, from which the general characteristics of the hybrid system are revealed and the optimum criteria of some important parameters are determined. Moreover, a multi-objective function is put forward to further subdivide the optimally operating regions according to the different requirements for the efficiency and power output. The influence of the irreversibilities on the performance of the hybrid system is discussed in detail. The results obtained here may provide some theoretical basis for the optimal design and operation of practical MCFC-heat engine hybrid systems.

ACKNOWLEDGEMENTS

This work has been supported by the National Natural Science Foundation (No. 51076134) and the Fundamental Research Fund for the Central Universities (No. 201112G006), People's Republic of China.

References

1. D. C. Huang, P. J. Yu, F. J. Liu, S. L. Huang, K. L. Hsueh, Y. C. Chen, C. H. Wu, W. C. Chang, F. H. Tsau, *Int. J. Electrochem. Sci.*, 6 (2011) 2551.
2. M. EL Sayed Youssef, K. E. AL-NAdi, M. H. Khalil, *Int. J. Electrochem. Sci.*, 5 (2010) 267.
3. Y. Kiros, *Int. J. Electrochem. Sci.*, 2 (2007) 285.
4. G. J. K. Acres, *J. Power Sources*, 100 (2001) 60.
5. A. Qi, B. Peppley, K. Karan, *Fuel Process. Technol.*, 88 (2007) 3.
6. G. Cacciola, V. Antonucci, S. Freni, *J. Power Sources*, 100 (2001) 67.
7. R. O'Hayre, S. W. Cha, W. Colella, F. B. Prinz, *Fuel Cell Fundamentals*. John Wiley & Sons. Inc., New York (2006).
8. P. Tomczyk, *J. Power Sources*, 160 (2006) 858.
9. A. Dicks, A. Siddle, *J. Power Sources*, 86 (2000) 316.
10. P. S. Pak, Y. D. Lee, K. Y. Ahn, *Energy*, 34 (2009) 1903.

11. R. Rashidi, P. Berg, I. Dincer, *Int. J. Hydrogen Energy*, 34 (2009) 4395.
12. P. Lunghi, R. Bove, U. Desideri, *J. Power Sources*, 118 (2003) 108.
13. V. Verda, F. Nicolin, *Int. J. Hydrogen Energy*, 35 (2010) 794.
14. F. Jurado, *J. Power Sources*, 111 (2002) 121.
15. Y. Zhao, J. Chen, *J. Power Sources*, 186 (2009) 96.
16. X. Zhang, J. Chen, *Int. J. Hydrogen Energy*, 35 (2010) 284.
17. X. Chen, B. Lin, J. Chen, *Energy Fuel*, 23 (2009) 6079.
18. D. Sánchez, R. Chacartegui, M. Torres, T. Sánchez, *J. Power Sources*, 192 (2009) 84.
19. P. Lunghi, S. Ubertini, U. Desideri, *Energy Convers. Manage.*, 42 (2001) 1657.
20. S. Ubertini, P. Lunghi, *Fuel Cells*. Wiley, New York (2003).
21. J. Palsson, A. Selimovic, L. Sjunnesson, *J. Power Sources*, 86 (2000) 442.
22. S. Bensaid, S. Specchia, F. Federici, G. Saracco, V. Specchia, *Int. J. Hydrogen Energy*, 34 (2009) 2026.
23. J. Brouwer, F. Jabbari, E. M. Leal, T. Orr, *J. Power Sources*, 158 (2006) 213.
24. M. Baranak, H. Atakül, *J. Power Sources*, 172 (2007) 831.
25. C. Y. Yuh, J. R. Selman, *J. Electrochem. Soc.*, 138 (1991) 3642.
26. H. Zhang, G. Lin, J. Chen, *Int. J. Hydrogen Energy*, 36 (2011) 4015.
27. R. H. Perry, C. H. Chilton, *Chemical engineering's handbook*, 5th ed. McGraw Hill Kogakusha, Ltd., Tokyo (1973).
28. Y. Zhao, C. Ou, J. Chen, *Int. J. Hydrogen Energy*, 33 (2008) 4161.
29. J. A. Dean, *Lange's Handbook of Chemistry*, 13th Ed. McGraw Hill Book Company, New York (1985).
30. H. Zhang, S. Su, G. Lin, J. Chen, *Int. J. Electrochem. Sci.*, 6 (2011) 2566.
31. H. Zhang, G. Lin, J. Chen, *Int. J. Hydrogen Energy*, 35 (2010) 10851.
32. A. Liu, Y. Weng, *J. Power Sources*, 195 (2010) 1872.
33. J. H. Koh, B. S. Kang, H. C. Lim, *AIChE J.*, 47 (2001) 1941.
34. A. Liu, Y. Weng, *J. Power Sources*, 195 (2010) 204.
35. S. Campanari, P. Chiesa, G. Manzolini, *Int. J. Greenhouse Gas Control*, 4 (2010) 441.
36. J. Chen, *J. Phys. D: Appl. Phys.*, 27 (1994) 1144.
37. M. Bojic, *Energy Convers. Manage.*, 38 (1997) 1877.
38. J. Chen, *J. Appl. Phys.*, 72 (1992) 3778.
39. A. Durmayaz, O. S. Sogut, B. Sahin, H. Yavuz, *Prog. Energy Combust. Sci.*, 30 (2004) 175.
40. S. Sieniutycz, *Prog. Energy Combust. Sci.*, 29 (2003) 193.
41. P. Holtappels, H. Mehling, S. Roehlich, S. S. Liebermann, U. Stimming, *Fuel Cells*, 5 (2005) 499.
42. P. G. Bavarsad, *Int. J. Hydrogen Energy*, 32 (2007) 4591.
43. Z. Yan, *J. Eng. Thermal. Energy Power*, 4 (1989) 1.
44. W. Na, B. Gou, *J. Power Sources*, 166 (2007) 411.
45. S. M. C. Ang, D. J. L. Brett, E. S. Fraga, *J. Power Sources*, 195 (2010) 2754.
46. H. Zhang, G. Lin, J. Chen, *Energy*, 36 (2011) 4327.